

Unveiling the basis of alkaline stability of an evolved versatile peroxidase

Verónica Sáez-Jiménez*, Sandra Acebes†‡, Eva García-Ruiz§, Antonio Romero*, Víctor Guallar†||, Miguel Alcalde¶, Francisco J. Medrano*, Angel T. Martínez* and Francisco J. Ruiz-Dueñas*¹

*Centro de Investigaciones Biológicas, CSIC, Ramiro de Maeztu 9, E-28040 Madrid, Spain

†Joint BSC-CRG-IRB Research Program in Computational Biology, Barcelona Supercomputing Center, Jordi Girona 29, E-08034 Barcelona, Spain

‡Anaxomics Biotech, Balmes 89, E-08008 Barcelona, Spain

§Department of Chemical and Biomolecular Engineering, University of Illinois at Urbana-Champaign, 600 South Mathews Avenue, Urbana, IL 61801, U.S.A.

||ICREA, Passeig Lluís Companys 23, E-08010 Barcelona, Spain

¶Institute of Catalysis and Petroleochemistry, CSIC, Marie Curie 2, Cantoblanco, E-28049 Madrid, Spain

A variant of high biotechnological interest (called 2-1B) was obtained by directed evolution of the *Pleurotus eryngii* VP (versatile peroxidase) expressed in *Saccharomyces cerevisiae* [García-Ruiz, González-Pérez, Ruiz-Dueñas, Martínez and Alcalde (2012) *Biochem. J.* **441**, 487–498]. 2-1B shows seven mutations in the mature protein that resulted in improved functional expression, activity and thermostability, along with a remarkable stronger alkaline stability (it retains 60% of the initial activity after 120 h of incubation at pH 9 compared with complete inactivation of the native enzyme after only 1 h). The latter is highly demanded for biorefinery applications. In the present study we investigate the structural basis behind the enhanced alkaline stabilization of this evolved enzyme. In order to do this, several VP variants containing one or several of the mutations present in 2-1B were expressed in *Escherichia coli*, and their alkaline stability and biochemical properties were determined. In addition, the crystal structures of 2-1B and one of

the intermediate variants were solved and carefully analysed, and molecular dynamics simulations were carried out. We concluded that the introduction of three basic residues in VP (Lys-37, Arg-39 and Arg-330) led to new connections between haem and helix B (where the distal histidine residue is located), and formation of new electrostatic interactions, that avoided the hexa-co-ordination of the haem iron. These new structural determinants stabilized the haem and its environment, helping to maintain the structural enzyme integrity (with penta-co-ordinated haem iron) under alkaline conditions. Moreover, the reinforcement of the solvent-exposed area around Gln-305 in the proximal side, prompted by the Q202L mutation, further enhanced the stability.

Key words: directed evolution, pH stability, structure–function relationships, versatile peroxidase.

INTRODUCTION

Lignin is the main reservoir of aromatic compounds in living organisms and a valuable feedstock for the sustainable production of chemicals and materials [1,2]. Owing to its aromatic and heterogeneous nature, lignin is highly resistant to chemical and biological degradation [3]. White-rot fungi produce ligninolytic peroxidases involved in lignin degradation, and they are the only organisms in Nature able to extensively mineralize lignin [4,5]. Ligninolytic peroxidases include three families: LiPs (lignin peroxidases) (EC 1.11.1.14), which oxidize high-redox-potential substrates through an exposed tryptophan radical formed by electron transfer to the haem [6]; MnPs (manganese peroxidases) (EC 1.11.1.13), which oxidize Mn^{2+} to Mn^{3+} at a specific manganese-binding site near one of the haem propionates [7,8]; and VPs (versatile peroxidases) (EC 1.11.1.16), which combine the catalytic properties of LiPs and MnPs (due to the simultaneous presence of the exposed tryptophan residue and the manganese-binding site, mentioned above) at the same time that they oxidize the typical substrates of GPs (generic peroxidases) (EC 1.11.1.7) at the main haem access channel [9,10].

The above enzymes have evolved to overcome the recalcitrant nature of lignin taking advantage of their high redox potential,

unspecific oxidation mechanism and other catalytic properties. Their use in industrial processes that require the oxidation of lignin and other phenolic and non-phenolic aromatic compounds and dyes is therefore very promising [11]. In this way, ligninolytic peroxidases could be used in the deconstruction of the lignocellulosic biomass and production of biofuels, materials and chemicals in lignocellulose biorefineries, in bioremediation processes for the treatment of recalcitrant dye wastes, or in bleaching applications in paper pulp manufacture [2,12,13]. However, there are some drawbacks that prevent the industrial application of these enzymes as they are produced in Nature. Among them, it is possible to mention their relative low stability towards some conditions of pH, temperature or hydrogen peroxide concentration, in which industrial processes are often carried out (including the alkaline conditions often used in lignocellulose processing) [2].

2-1B is an enzyme variant obtained by directed evolution of the VP from *Pleurotus eryngii* in *Saccharomyces cerevisiae* [14]. During the evolutionary process, seven mutations were introduced in the sequence of mature VP. As a consequence, 2-1B showed enhanced expression levels, increased thermostability and alkaline stability, and improved oxidation of some substrates. In the present study, five VP variants containing one or several

Abbreviations: ABTS, 2,2'-azino-bis-(3-ethylbenzothiazoline-6-sulfonic acid); B&R, Britton–Robinson; CDS, coding DNA sequence; CT, charge transfer; DMP, 2,6-dimethoxyphenol; GP, generic peroxidase; LiP, lignin peroxidase; MnP, manganese peroxidase; RB5, Reactive Black 5; VA, veratryl alcohol; VP, versatile peroxidase.

¹ To whom correspondence should be addressed (email fjruiz@cib.csic.es).

The co-ordinates and structure factors for the 2-1B and EH3 variants of the *Pleurotus eryngii* VP have been deposited in the PDB under codes 5FNB and 5FNE respectively.

Table 1 Seven mutations present in 2-1B and their combination in the five intermediate variants analysed

Variant	Mutation
2-1B	E37K/H39R/V160A/T184M/Q202L/D213A/G330R
H39R	H39R
EG	E37K/G330R
EHG	E37K/H39R/G330R
EHGQ	E37K/H39R/Q202L/G330R
EHGT	E37K/H39R/T184M/G330R

of the mutations present in 2-1B were designed, heterologously expressed, and their biochemical properties carefully evaluated, at the same time that the crystal structures of two of the most relevant variants were solved and used in molecular simulations. The final objective was to understand how the substitutions introduced by directed molecular evolution modulate the alkaline stability and catalytic properties of the enzyme, with the aim of using this information in future peroxidase engineering work.

MATERIALS AND METHODS

Chemicals

IPTG, DTT, EDTA, haemin, oxidized glutathione, VA (veratryl alcohol), manganese(II) sulfate, RB5 (Reactive Black 5), DMP (2,6-dimethoxyphenol), sodium tartrate and other chemicals were purchased from Sigma–Aldrich; urea and hydrogen peroxide were from Merck; and ABTS [2,2'-azinobis-(3-ethylbenzothiazoline-6-sulfonic acid)] was from Roche.

Directed mutagenesis

All VP variants except 2-1B (Table 1) were produced using the QuikChange™ Site-Directed Mutagenesis kit (Stratagene). Each mutation was introduced by PCR using the expression plasmid pFLAG1 (International Biotechnologies) containing the CDS (coding DNA sequence) of *P. eryngii* VPL (allelic variant VPL2; GenBank® accession number AF007222), named pFLAG1-VPL2, or the same plasmid containing already mutated CDSs as templates and two primers, a direct and a reverse primer designed complementary to opposite strands of the same DNA region containing the desired mutation. PCRs were carried out in an Eppendorf Mastercycler Pro S using 10 ng of template DNA, 250 μM of each dNTP, 125 ng of both direct and reverse primers, 2.5 units of Pfu Turbo AD polymerase (Stratagene) and the manufacturer's reaction buffer. Reaction conditions were as follows: (i) a 'hot start' of 95 °C for 1 min; (ii) 18 cycles at 95 °C for 50 s, 55 °C for 50 s and 68 °C for 10 min; and (iii) a final cycle at 68 °C for 10 min. Clones harbouring mutations were transformed into *Escherichia coli* DH5α. One positive clone of each variant was selected, sequenced (PerkinElmer ABI Prism 377) and checked to confirm that the desired mutations had been properly introduced.

Heterologous expression

Wild-type recombinant (hereinafter referred to as native) VP and its directed variants were expressed in *E. coli* W3110 after transformation with the corresponding plasmids. The gene encoding the 2-1B variant was obtained by digesting the plasmid used for *S. cerevisiae* expression [14], cloned into pFLAG1

(resulting in the pFLAG-VPL2-2-1B construct) and transformed into *E. coli* W3110 for expression.

Cells were grown in Terrific broth [15] at 37 °C until reaching a D_{500} of ~1 (~3 h). Then protein expression was induced with 1 mM IPTG and cells were grown for a further 4 h. The apoenzyme was produced as inclusion bodies and was recovered in a 50 mM Tris/HCl (pH 8.0) solution containing 8 M urea, 1 mM EDTA and 1 mM DTT. The subsequent *in vitro* folding of the solubilized apoenzyme was carried out in a solution of 0.16 M urea, 20 μM haemin, 5 mM CaCl₂, 0.1 mM DTT, 0.5 mM oxidized glutathione and 0.1 mg/ml protein concentration in 20 mM Tris/HCl buffer, at pH 9.5, at room temperature overnight. The refolded enzyme was purified by Resource-Q chromatography using a 0–0.3 M NaCl gradient (2 ml/min for 20 min) in 10 mM sodium tartrate (pH 5.5) containing 1 mM CaCl₂. Finally, the purified enzyme was dialysed against 10 mM sodium tartrate (pH 5). The proteins showed Reinheitszahl values (R_z , A_{407}/A_{280}) of ~4 confirming their high purity. Their UV-visible spectra in the 300–700 nm range confirmed that they were correctly folded [16]. Enzyme concentrations were determined from the Soret absorbance ($\epsilon_{407} = 150 \text{ mM}^{-1} \cdot \text{cm}^{-1}$) [17].

pH stability studies

Native VP and its directed variants (1 μM) were incubated at different pH values (from 2 to 9) in 0.1 M B&R (Britton–Robinson) buffer (0.1 M phosphoric acid, 0.1 M boric acid and 0.1 M acetic acid; pH adjusted with NaOH) [18] at 4 °C for 120 h. At different times (1 min, 1 h, 4 h, 24 h and 120 h), aliquots were taken and their residual activity was evaluated by measuring the oxidation of ABTS (2 mM) using 0.1 mM H₂O₂ and 0.01 μM of enzyme in 0.1 M sodium tartrate (pH 3.5). The activity obtained from samples incubated for 1 min at pH 5 was taken as reference (maximum activity) to calculate the percentage of residual activity. Native VP and those variants showing improved alkaline stability (2-1B, EHG and EHGQ) (8 μM) were incubated at pH 5 or pH 8 in 0.1 M B&R buffer for 120 h at 4 °C, and their electronic absorption spectra (in the 300–800 nm range) were recorded using an Agilent 8453 diode array UV-visible spectrophotometer.

Kinetic constants

Oxidation of Mn²⁺ (Mn³⁺–tartrate complex $\epsilon_{238} = 6500 \text{ M}^{-1} \cdot \text{cm}^{-1}$) was estimated at pH 5; that of VA (veratraldehyde $\epsilon_{310} = 9300 \text{ M}^{-1} \cdot \text{cm}^{-1}$) at pH 3; and those of RB5 ($\epsilon_{598} = 30000 \text{ M}^{-1} \cdot \text{cm}^{-1}$), ABTS (cation radical $\epsilon_{436} = 29300 \text{ M}^{-1} \cdot \text{cm}^{-1}$) and DMP (coerulignone dimeric product $\epsilon_{469} = 55000 \text{ M}^{-1} \cdot \text{cm}^{-1}$) at pH 3.5. All enzymatic activities were measured as initial velocities taking linear increments of absorbance due to the appearance of the reaction product (decreases in the case of RB5). Reactions were performed in 0.1 M tartrate buffer, at 25 °C, in the presence of 0.1 mM H₂O₂ using a variable-wavelength Shimadzu UV-1800 spectrophotometer.

Steady-state kinetic constants were calculated from the estimated oxidation of increasing substrate concentrations until enzyme saturation was observed. Values and standard errors for affinity constant (Michaelis constant, K_m) and maximal enzyme turnover (catalytic constant, k_{cat}) were obtained fitting the experimental measurements to the Michaelis–Menten model using SigmaPlot 12.0 software. Fitting of these constants to the normalized equation $v = (k_{cat}/K_m)[S]/(1 + [S]/K_m)$, where [S] is the substrate concentration, yielded the catalytic efficiency values (k_{cat}/K_m) with their corresponding standard errors.

Crystallization, data collection and crystal structure determination

Crystallization trials were carried out by the sitting-drop vapour-diffusion method, using 96-well MRC2 plates with 50 μ l of reservoir solution and the commercially available screenings from Emerald (Wizard classic crystallization screens I, II and III) and Jena Biosciences (JBScreen Classic Kits 1-10). Drops consisted of 0.2 μ l of protein solution (10 mg/ml in 10 mM sodium tartrate buffer at pH 5.0) and 0.2 μ l of reservoir solution. Crystallization was carried out at 22 °C. Crystals of 2-1B were obtained in 0.1 M Tris/HCl (pH 7.8), 5% PEG3350, 1.25 M (NH₄)₂SO₄ and 7.5% glycerol; and cryoprotected raising the amount of glycerol up to 30%. Crystals of EHG were obtained in 0.1 M sodium acetate (pH 4.5), 1.26 M (NH₄)₂SO₄ and 0.2 M NaCl; and cryoprotected with 0.8 M Li₂SO₄.

Crystals were mounted in nylon loops and flash-frozen in liquid nitrogen in the mother liquor containing the cryoprotectant indicated above. All diffraction data were obtained at 100 K. X-ray diffraction intensities were collected at the X06DA beamline at the Swiss Light Source (Villigen, Switzerland) using a wavelength of 1.0000 Å (1 Å = 0.1 nm). Diffraction data were indexed, integrated, merged and scaled using the program XDS [19]. Data collection statistics are shown in Table 2.

The structures of the two VP variants were solved by molecular replacement using the crystal structure of *P. eryngii* VPL (PDB code 3FMU) as the search model and the program PHASER implemented in the PHENIX package [20]. The final models were obtained by consecutive rounds of refinement, performed with the PHENIX package; followed by manual model building, performed with Coot [21] using σ_A weighted $2F_o - F_c$ and $F_o - F_c$ electron density maps. Solvent molecules were introduced in the structure automatically in the refinement as implemented in the PHENIX package and visually inspected. A total of 5% of reflections was used to calculate the R_{free} value throughout the refinement process. The structures were validated using MolProbity [22,23]. Refinement and final model statistics are summarized in Table 2. The co-ordinates and structural factors have been deposited with the PDB. All Figures were produced with PyMOL (<http://www.pymol.org/>).

Molecular dynamics

Structural and dynamic differences between native VP and its 2-1B variant were studied by MD simulations. Hydrogen addition, ligand optimization, completion of the two terminal residues and protonation state adjustment of ionizable residues (glutamate, histidine and aspartate) in both crystal structures were performed with the protein preparation wizard [24] at pH 8. MD simulations were then produced using the Desmond software and its Maestro interface from Schrodinger. Enzymes were solvated in an orthorhombic box with at least 10 Å from the protein surface, followed by NaCl addition for an ionic force of 0.15 M. The default relaxation protocol in Desmond was performed followed by a 20 ns trajectory production with the OPLS-2005 [25] force field at 300K. The NPT ensemble with Nose-Hoover thermostat [26] and a Martyna-Tobias-Klein barostat [27] were employed.

RESULTS

pH stability of the different variants

VP 2-1B (containing E37K/H39R/V160A/T184M/Q202L/D213A/G330R mutations) expressed in *E. coli* showed improved alkaline stability (Figure 1D) compared with native VP (Figure 1A). After 24 and 120 h of incubation at pH 8, it retained

Table 2 Crystallographic data collection and refinement statistics of VP EHG and VP 2-1B

Values in parentheses correspond to the highest resolution layer.

	EHG	2-1B
Data collection		
Space group	$P2_12_12$	$P2_12_12_1$
Cell constants	$a = 55.2, b = 104.3,$ $c = 76.7 \text{ \AA}$	$a = 55.2, b = 106.3,$ $c = 107.9 \text{ \AA}$
Resolution range (Å)	50.00–1.70 (1.89–1.70)	50.00–2.00 (2.12–2.00)
Number of total reflections	646657	577925
Number of unique reflections	49391	43670
R_{merge} (%)	19.2 (145.6)	32.5 (171.0)
Completeness (%)	99.6 (97.6)	99.2 (96.9)
$\langle I/\sigma(I) \rangle$	11.9 (1.9)	8.7 (1.5)
CC(1/2)	99.7 (70.7)	99.2 (63.2)
Solvent content (%) / Matthews coefficient	55.3/2.75	37.5/1.97
Subunits per asymmetric unit	1	2
Wilson B factor (Å ²)	25.0	27.0
Refinement		
Resolution range	50.0–1.70 Å	50.0–2.00 Å
Working reflections	49358	43615
R_{work}/R_{free}	19.7/22.8%	18.6/23.6%
Protein atoms (non-hydrogen)	2423	4764
Haem group	1	2
Ca ²⁺	2	4
Water molecules	362	266
SO ₄ ions	5	1
Mean B factors (Å ²)		
Protein atoms (non H)	20.4	20.7
Heme group	16.2	16.2
Ca ²⁺	14.5	14.8
Water molecules	29.1	24.2
SO ₄ ions	43.3	25.0
Deviations from ideality		
RMSD bond lengths	0.006 Å	0.008 Å
RMSD angles	0.886°	0.928°
Ramachandran plot statistics		
Preferred (%)	98.17	98.44
Allowed (%)	1.83	1.41
Outliers (%)	0.00	0.16
PDB code	5FNE	5FNB

82% and 78% of residual activity respectively, whereas native VP was fully inactivated. Moreover, after 1 h of incubation at pH 9, native VP retained only 5% of the initial activity, whereas 2-1B maintained 36% of activity. The differences in stability between both enzymes at neutral and most acidic pH conditions (in the pH 3.5–7 range) were minimal, and 2-1B was less stable at the lowest pH value (pH 3) assayed.

To analyse the effect of each of the individual mutations in 2-1B, and the effect of combining them, several single and multiple VP variants were designed (Table 1), expressed in *E. coli* and characterized. The H39R variant showed high instability at acidic and alkaline pH values compared with native VP (Figure 2A). Native VP maintained ~90% of the initial activity in the pH 4–7 range after 120 h of incubation, whereas H39R only showed 41%, 68% and 21% activity at pH 4, 5 and 6 respectively (and no activity at pH 7). The following VP variant analysed, EG containing mutations E37K/G330R, exhibited similar pH stability to native VP and no improvement in the alkaline range was observed (Figure 2B).

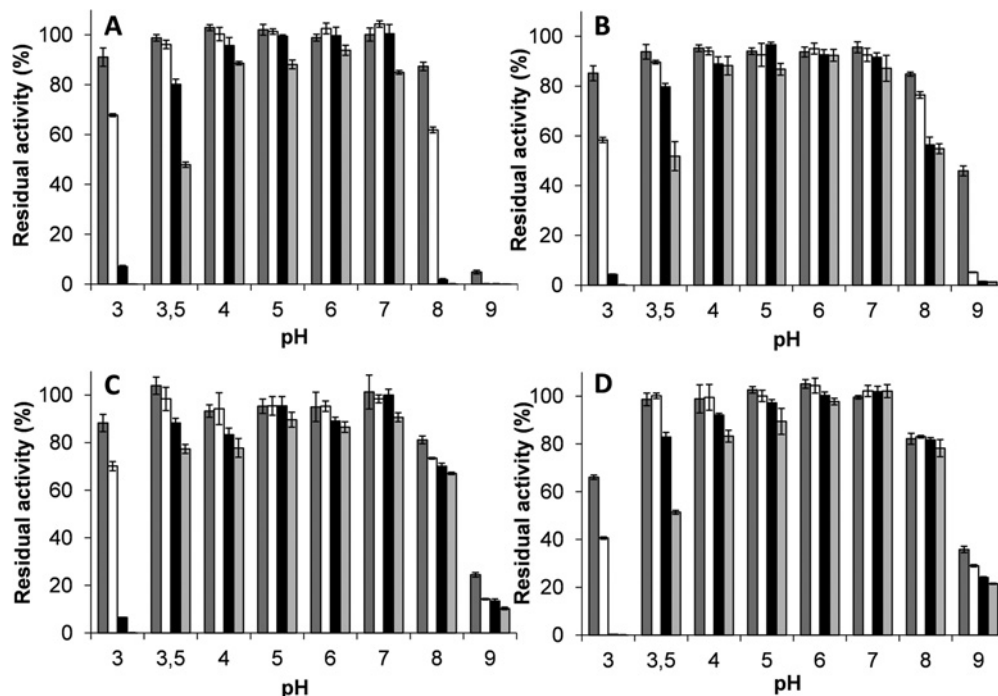


Figure 1 pH stability of native VP, and EHG, EHGQ and 2-1B mutated variants

Residual activities of VP (A), and the EHG (B), EHGQ (C) and 2-1B (D) variants, after 1 h (dark grey bars), 4 h (white bars), 24 h (black bars) and 120 h (light grey bars) of incubation in 0.1 M B&R buffer at different pH values (3–9) and 4 °C. Residual activity measured as ABTS (2 mM) oxidation in 0.1 M sodium tartrate (pH 3.5) using 0.01 μ M enzyme and 0.1 mM H₂O₂. Results are means \pm 95% confidence limits for replicate assays. See Table 1 for the mutations present in each of the variants.

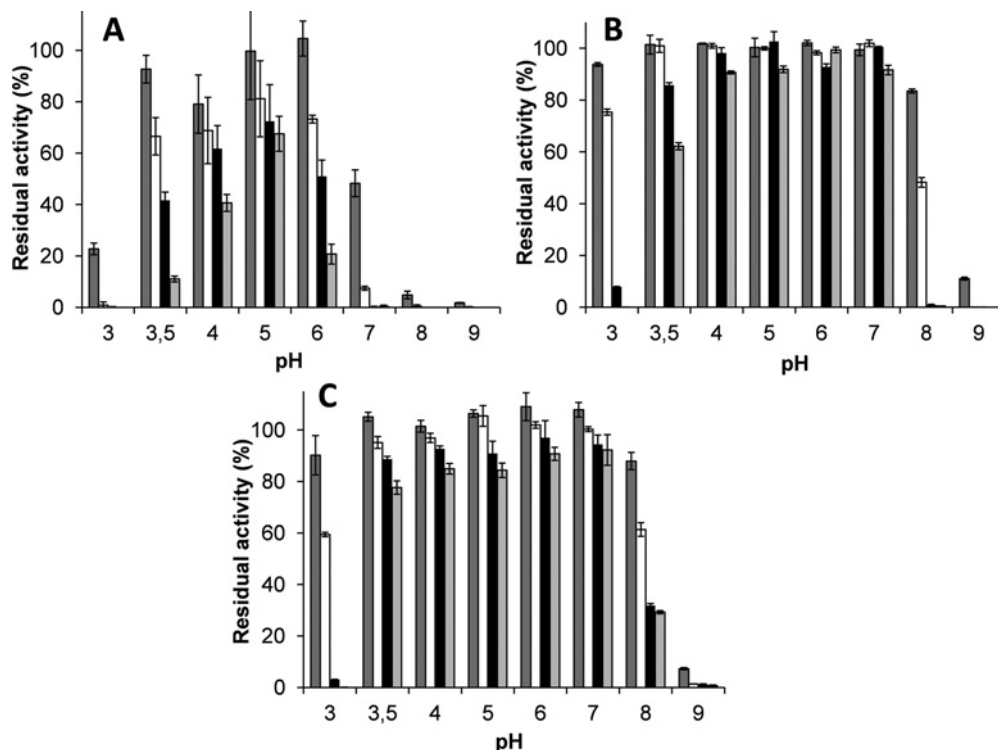


Figure 2 pH stability of H39R, EG and EHG VP variants

Residual activities of H39R (A), EG (B) and EHG (C) after incubation in 0.1 M B&R buffer at different pH values (3–9) and 4 °C for 1 h (dark grey bars), 4 h (white bars), 24 h (black bars) and 120 h (light grey bars). Residual activity measured as ABTS (2 mM) oxidation in 0.1 M sodium tartrate (pH 3.5) using 0.01 μ M enzyme and 0.1 mM H₂O₂. Results are means \pm 95% confidence limits for replicate assays. See Table 1 for the mutations present in each of the variants.

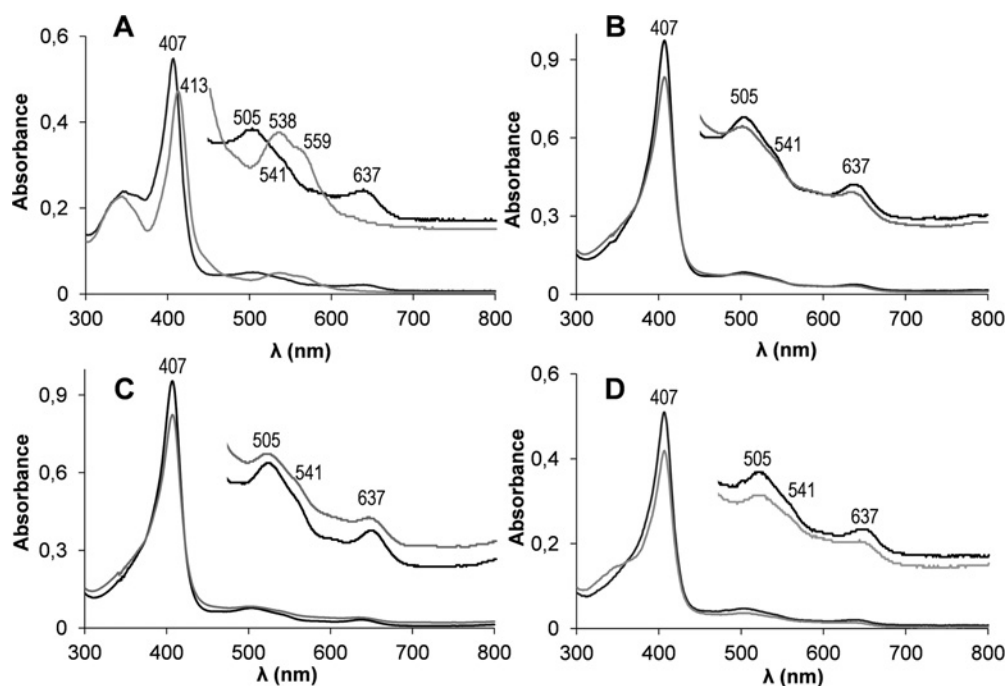


Figure 3 Electronic absorption spectra of native VP and variants after treatments at pH 5 and pH 8

UV–visible spectra of native VP (A), and the EHG (B), EHGQ (C) and 2-1B (D) variants incubated for 120 h in 0.1 M B&R buffer at pH 5 (black) and pH 8 (grey) at 4 °C. Amplified ($\times 5$) 450–800 nm regions are shown. Main maxima are indicated.

Surprisingly, the EHG variant, which combined the mutations of the two variants analysed previously (E37K/H39R/G330R), displayed an increase in the alkaline stability compared with native VP (Figure 1B). This triple variant maintained 55 % of the initial activity after 120 h of incubation at pH 8, whereas native VP not only showed no activity under these conditions, but was already inactivated after 24 h of incubation (Figure 1A). In a similar way, after 1 h of incubation at pH 9, EHG exhibited 46 % of the initial activity, whereas native VP only retained 5 %. Moreover, this variant maintained a similar stability to that of native VP at acidic and neutral pH values. However, the values of pH stability observed for EHG were not as high as those obtained for 2-1B, which retained 78 % of activity after 120 h of incubation at pH 8 (Figure 1D).

The next VP variant analysed was EHGQ (E37K/H39R/Q202L/G330R), which harboured the three mutations of EHG plus the Q202L mutation, also found in 2-1B. EHGQ showed 67 % of residual activity after 120 h of incubation at pH 8 (Figure 1C), a value higher than that of EHG (55 % of activity). EHGQ also retained a low percentage of the initial activity (24 %) after 1 h of incubation at pH 9 compared with native VP, which was completely inactivated. Therefore, it was determined that the Q202L substitution also contributed to the enhancement of the pH stability in 2-1B. As described previously for EHG, its stability at neutral and acidic pH was similar to that of the native VP.

The last variant tested, EHGT (E37K/H39R/T184M/G330R), harboured the three mutations introduced in EHG plus the T184M mutation, also found in 2-1B. After 120 h at pH 8, EHGT displayed 30 % of the initial activity (Figure 2C) compared with 55 % of activity retained by EHG. In consequence, we concluded that the T184M substitution did not contribute to the alkaline stability of 2-1B.

pH effect on the UV–visible spectra

The electronic absorption spectra of native VP and its variants were recorded after incubation at alkaline pH 8, and at pH 5 at which all of them are stable, to check the eventual modification of the haem interactions with its protein environment. As expected, all of the spectra at pH 5 exhibited a Soret maximum at 407 nm, maxima at 505 nm and 637 nm corresponding to ligand-to-metal charge transfer bands (CT2 and CT1 respectively), and the β band at 541 nm (Figure 3, black lines), which correspond to the typical spectrum of the ferric enzyme with high-spin penta-co-ordinated haem iron.

However, the spectrum of native VP after incubation at pH 8 suffered important changes (Figure 3A, grey lines). The Soret maximum was red-shifted to 413 nm and showed less intensity, the CT bands at 505 nm and 637 nm disappeared and a new maximum rose at 538 nm (β band) together with a shoulder at 559 nm (α band). In contrast, 2-1B mostly preserved the spectrum when incubated at pH 8 (Figure 3D, grey lines), maintaining the Soret maximum at 407 nm, as well as the CT1, CT2 and β bands at 637, 505 and 541 nm respectively. In the same way, the EHG and EHGQ variants also preserved the ferric high-spin haem spectrum with all maxima unaffected (Figures 3B and 3C, grey lines, respectively).

Catalytic properties

Different substrates are oxidized at specific VP sites: (i) high-redox-potential VA and RB5 are oxidized at the catalytic tryptophan residue; (ii) low-redox-potential ABTS and DMP are oxidized both at the catalytic tryptophan residue (high-efficiency site) and at the haem channel in direct contact with the haem edge (low-efficiency site); and (iii) Mn^{2+} is oxidized at the

Table 3 Kinetic constants, k_{cat} (s^{-1}), K_{m} (μM) and $k_{\text{cat}}/K_{\text{m}}$ ($\text{s}^{-1} \cdot \text{mM}^{-1}$), for oxidation of VA, RB5, Mn^{2+} , ABTS and DMP by native VP, 2-1B and three intermediate variants (see Table 1)

Reactions were carried out at 25 °C in 0.1 M sodium tartrate (pH 3 for VA, pH 5 for Mn^{2+} and pH 3.5 for RB5, ABTS and DMP). Results are means \pm 95% confidence limits of replicate assays. ABTS and DMP oxidation showed biphasic kinetics enabling calculation of two sets of constants (for high- and low-efficiency sites). ND, not determined because the kinetic curve of the high-efficiency site overlapped with that of the low-efficiency site.

		VP	EHG	EHGQ	EHGT	2-1B
VA	k_{cat}	5.8 \pm 0.1	5.2 \pm 0.1	4.4 \pm 0.04	5.9 \pm 0.1	3.8 \pm 0.1
	K_{m}	2600 \pm 190	2110 \pm 150	1780 \pm 60	5910 \pm 190	2710 \pm 270
	$k_{\text{cat}}/K_{\text{m}}$	2.2 \pm 0.1	2.5 \pm 0.1	2.5 \pm 0.1	1.0 \pm 0.1	1.4 \pm 0.1
RB5	k_{cat}	5.5 \pm 0.3	7.8 \pm 0.4	6.7 \pm 0.3	5.1 \pm 0.1	6.7 \pm 0.3
	K_{m}	3.4 \pm 0.3	4.3 \pm 0.5	3.5 \pm 0.3	2.4 \pm 0.1	7.6 \pm 0.6
	$k_{\text{cat}}/K_{\text{m}}$	1.6 \pm 0.1	1.8 \pm 0.1	1.1 \pm 0.1	2.2 \pm 0.1	0.8 \pm 0.1
ABTS (high efficiency)	k_{cat}	8.1 \pm 0.2	8.3 \pm 0.3	7.2 \pm 0.3	39 \pm 7	ND
	K_{m}	3.0 \pm 0.2	2.6 \pm 0.2	2.3 \pm 0.2	13 \pm 3	ND
	$k_{\text{cat}}/K_{\text{m}}$	2700 \pm 140	3100 \pm 180	3200 \pm 150	3050 \pm 160	ND
ABTS (low efficiency)	k_{cat}	208 \pm 6	89 \pm 2	90 \pm 2	117 \pm 2	234 \pm 8
	K_{m}	1020 \pm 70	400 \pm 40	280 \pm 20	61 \pm 3	98 \pm 9
	$k_{\text{cat}}/K_{\text{m}}$	204 \pm 10	219 \pm 15	320 \pm 20	1920 \pm 70	2370 \pm 150
DMP (high efficiency)	k_{cat}	7.1 \pm 0.1	2.9 \pm 0.1	4.1 \pm 0.1	6.3 \pm 0.3	2.9 \pm 0.4
	K_{m}	38 \pm 4	17 \pm 2	16 \pm 3	11 \pm 2	27 \pm 7
	$k_{\text{cat}}/K_{\text{m}}$	186 \pm 16	168 \pm 18	250 \pm 38	559 \pm 80	112 \pm 18
DMP (low efficiency)	k_{cat}	30 \pm 1	40 \pm 4	56 \pm 4	46 \pm 2	91 \pm 2
	K_{m}	10500 \pm 400	34500 \pm 6050	34100 \pm 5290	3070 \pm 420	7470 \pm 380
	$k_{\text{cat}}/K_{\text{m}}$	2.8 \pm 0.1	1.1 \pm 0.1	1.6 \pm 0.1	15 \pm 2	12 \pm 1
Mn^{2+}	k_{cat}	211 \pm 4	208 \pm 2	188 \pm 2	160 \pm 4	143 \pm 3
	K_{m}	130 \pm 11	7020 \pm 190	6790 \pm 200	5590 \pm 371	5710 \pm 350
	$k_{\text{cat}}/K_{\text{m}}$	1640 \pm 130	30 \pm 1	28 \pm 1	29 \pm 1	25 \pm 1

Mn^{2+} -binding site, in direct contact with a haem propionate. The steady-state kinetic constants for the oxidation of the above five substrates by native VP and four variants were measured (Table 3).

In general, the oxidation of substrates at the catalytic tryptophan residue was not affected by the substitutions introduced in 2-1B, since the kinetic constants for the oxidation of VA, RB5, and ABTS and DMP (in the high-efficiency site) were mostly unaltered in this and the other variants. The only exception was EHGT which exhibited a 3-fold higher catalytic efficiency (559 $\text{s}^{-1} \cdot \text{mM}^{-1}$) for DMP oxidation, compared with that of native VP (186 $\text{s}^{-1} \cdot \text{mM}^{-1}$), due to a decrease in the affinity constant (K_{m}).

Mn^{2+} oxidation was impaired in 2-1B and the rest of analysed variants since their efficiency values were decreased \sim 60-fold, changing from 1640 $\text{s}^{-1} \cdot \text{mM}^{-1}$ in native VP to 25–30 $\text{s}^{-1} \cdot \text{mM}^{-1}$ in the variants. The decline in oxidation of Mn^{2+} was mainly due to loss of substrate affinity since the K_{m} values for Mn^{2+} were substantially (40–50-fold) higher than for the native VP enzyme (Table 3).

Interestingly, the oxidation of ABTS and DMP at the low-efficiency site was improved in 2-1B and EHGT. The efficiency for the oxidation of ABTS showed a 9–12-fold increase in both variants, mainly due to a reduction in the K_{m} values. In a similar way, the efficiency in the oxidation of DMP exhibited a 5-fold increase. In EHGT, this improvement was mainly due to the decrease in the K_{m} . However, in 2-1B, a decrease in the K_{m} value combined with an increase in the k_{cat} was observed.

In contrast with the results obtained for EHGT, EHG showed no improvement in ABTS and DMP oxidation. Since the only difference between these two variants is the T184M mutation present in EGHT, it was concluded that this substitution is involved in the improved oxidation of low-redox-potential substrates by EGHT (and probably by 2-1B).

Analysis of crystal structures

The crystal structures of 2-1B and EHG were obtained, analysed and compared with that of native VP (PDB code 2BOQ) [34] to explain, from a structural point of view, both the enhanced alkaline stability and the modified catalytic properties of these variants. The simultaneous presence of H39R, E37K and G330R mutations was a determinant for the higher alkaline stability found in 2-1B. Residues 37 and 39 are partially solvent-exposed, close to the haem (at 7.1 and 3.3 Å respectively in the native VP structure) (Figure 4A) and close to the Mn^{2+} -binding site (formed by Glu-36, Glu-40 and Asp-175). They belong to helix B, which is located directly above the haem and harbours the distal histidine (His-47) and the distal arginine (Arg-43) that are involved in catalysis. Moreover, the distal histidine is involved in the hexa-co-ordination of the haem iron observed at alkaline pH. The new Arg-39 in EHG and 2-1B (Figures 4C, 4D and 4E) showed a different orientation of its side chain relative to the position of His-39 in native VP (Figure 4B). The new orientation enabled the formation of a new hydrogen bond with the distal propionate of the haem, with this interaction being absent from native VP. Instead, in VP, His-39 formed two hydrogen bonds with Cys-34 and Pro-190, which were lost in the improved variants.

The E37K substitution changed an acidic residue for a basic one. The new lysine residue forms electrostatic interactions with Glu-40 in 2-1B (Figure 4D) and with Glu-36 and Glu-83 in EHG (Figure 4C). In contrast, the side chain of Glu-37 in VP does not make this type of interaction (Figure 4B). On the other hand, Glu-37 is close (<7 Å) to several acidic residues (such as Glu-40 and Glu-36 on helix B, Glu-83 on helix C, Glu-26 on helix A, and Asp-30 and Asp-175 on two loops). Therefore the introduction of the new Lys-37 in 2-1B and EHG variants contributed to reduce the putative destabilizing acid–acid interactions in the region where this mutation is located.

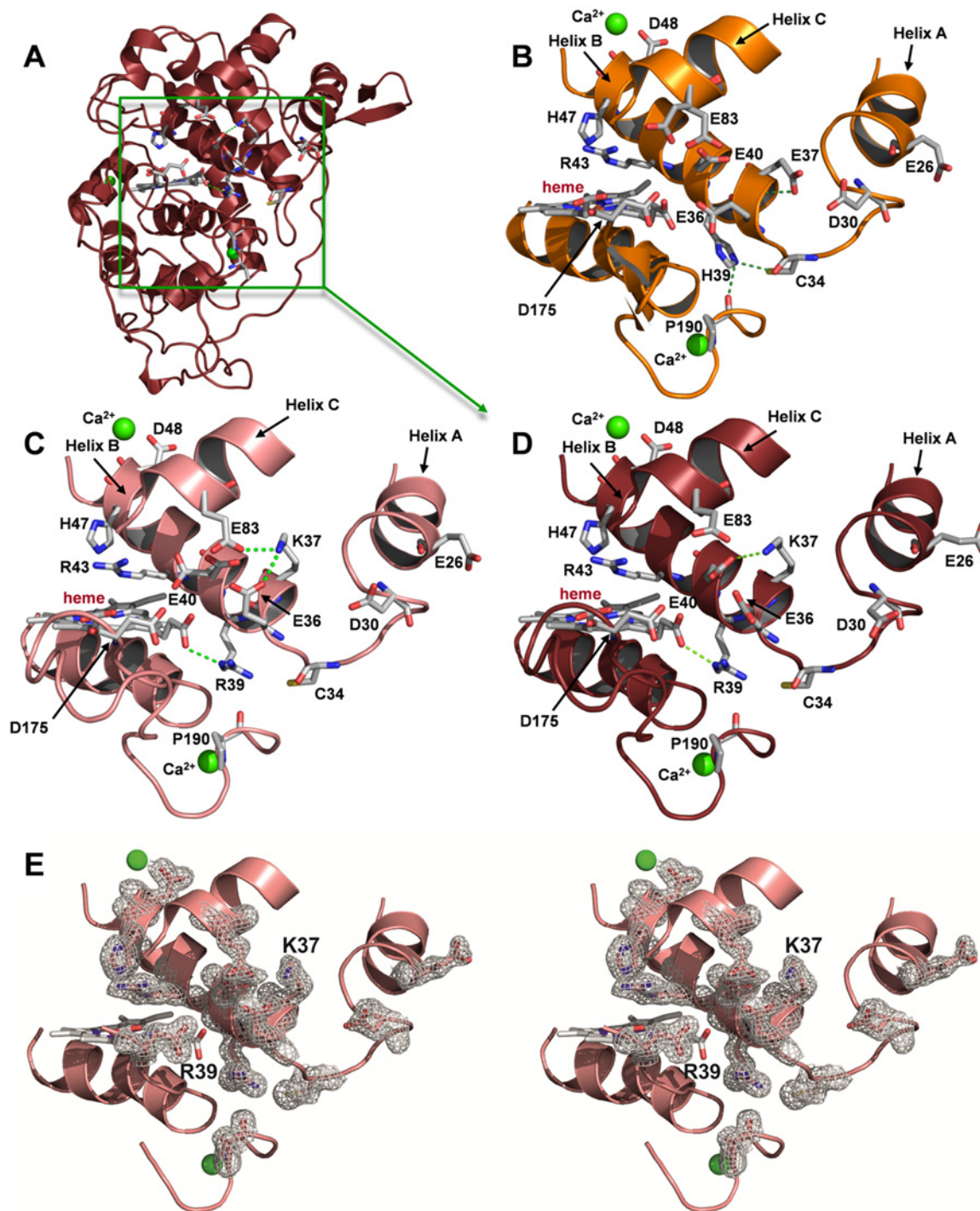


Figure 4 E37K and H39R mutations in 2-1B and EHG crystal structures

Crystal structure of 2-1B (A) with details of the region in front of the haem propionates in native VP (B) and the EHG (C) and 2-1B (D) variants showing the haem, the mutated residues at positions 37 and 39, and other surrounding residues [in CPK (Corey–Pauling–Koltun) colours]; and a stereo view of this region in EHG (E) showing the $(2F_o - F_c)$ electron density map, contoured at 1.0σ , of the same amino acid residues depicted in (C). 2-1B showed the same electron density (not shown). Hydrogen bonds are shown as green dashed lines, Ca^{2+} ions are shown as green spheres and secondary structure is shown as a coloured cartoon.

G330R was also involved in the pH-stability improvement of 2-1B. This is the penultimate residue in the VP C-terminal tail, and its position could not be determined in the crystals of native VP and its mutated variants owing to the high mobility of this area. For this reason, we could not verify in which way this mutation

contributes to enhance the stability. Nonetheless, it is interesting to note that residue 330 is close to residues 37 and 39, all of them around the Mn^{2+} -binding site.

Q202L, at the bottom of the molecule (Figure 5A) where the mutations V160A, T184M and D213A are also located

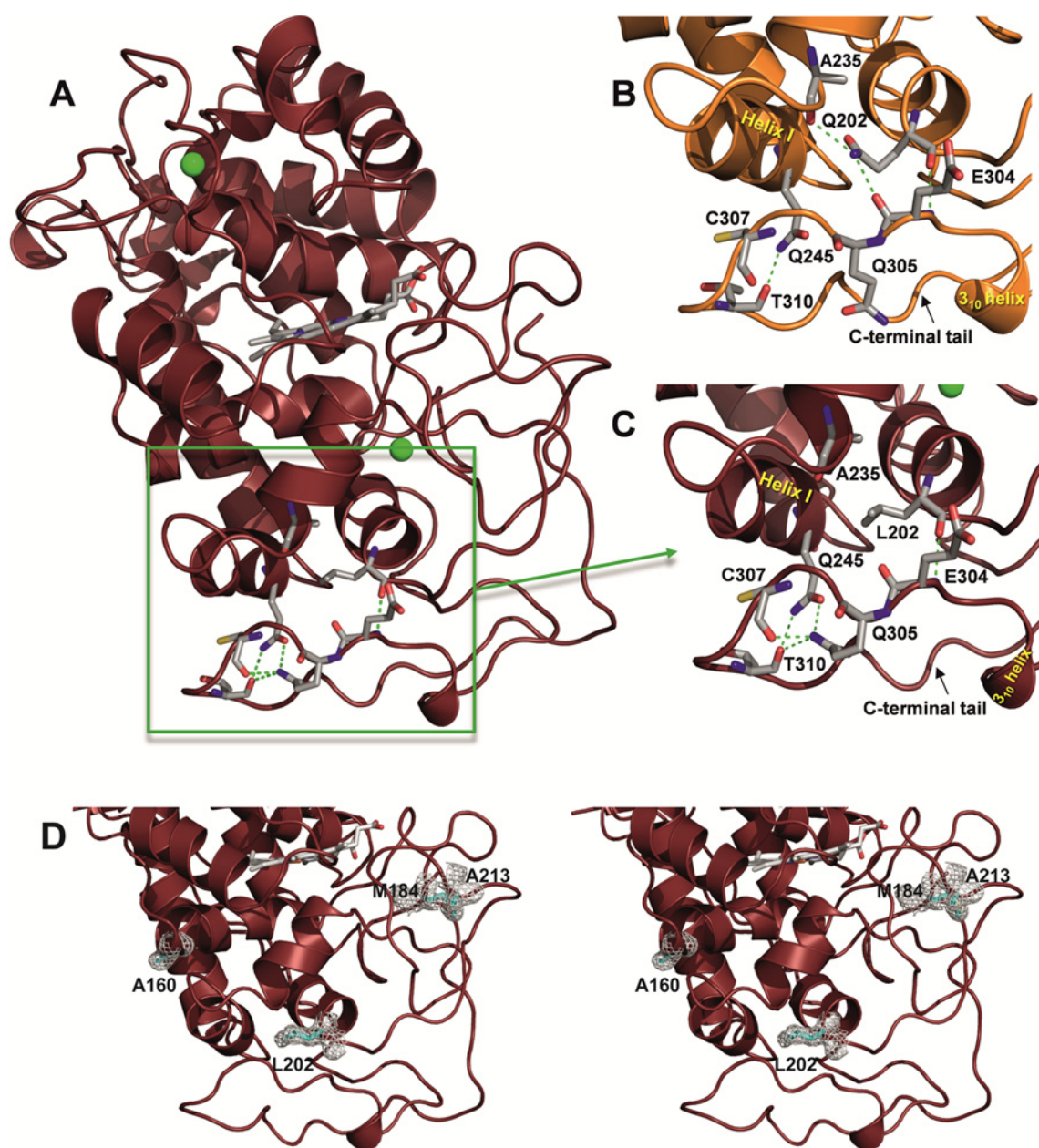


Figure 5 Q202L mutation in 2-1B crystal structure

Crystal structure of 2-1B (A) with a detail of the region around residue 202 in native VP (B) and the 2-1B (C) variant; and a stereo view of this region in 2-1B (D) showing the ($2F_o - F_c$) electron density map, contoured at 1.0σ , of the mutated residues at positions 160, 184, 202 and 213. Analysed residues are shown as CPK (Corey–Pauling–Koltun) sticks, hydrogen bonds are shown as green dashed lines, Ca^{2+} ions are shown as green spheres and secondary structure is shown as a coloured cartoon.

(Figure 5D), was the last mutation identified as stabilizing VP under alkaline conditions. The introduction of Leu-202 in 2-1B led to the disappearance of two hydrogen bonds present in native VP, one with Ala-235 and other with Glu-304 (Figures 5B and 5C). As a consequence, the position of the side chain of some surrounding residues changed in the 2-1B variant, especially that of Gln-305 forming three new interactions with Gln-245, Cys-307 and Thr-310 in 2-1B. These interactions reinforced and joined two solvent-exposed regions of the protein: (i) the helix I; and (ii) the loop between a 3_{10} helix (from Leu-300 to Asp-302) and the C-terminal tail. None of these interactions appeared in native VP.

Regarding the structural Ca^{2+} ions, described as essential for pH stability, both of them appeared in the 2-1B and EHG structures co-ordinated in the same way as in the native VP.

Finally, the T184M mutation was analysed in the 2-1B structure since it was involved in the enhanced oxidation of ABTS and DMP at the low-efficiency site. Residue 184 is solvent-exposed and located below the Mn^{2+} -binding site. No significant differences were observed between native VP and 2-1B in either the position of the surrounding residues or the interactions between them.

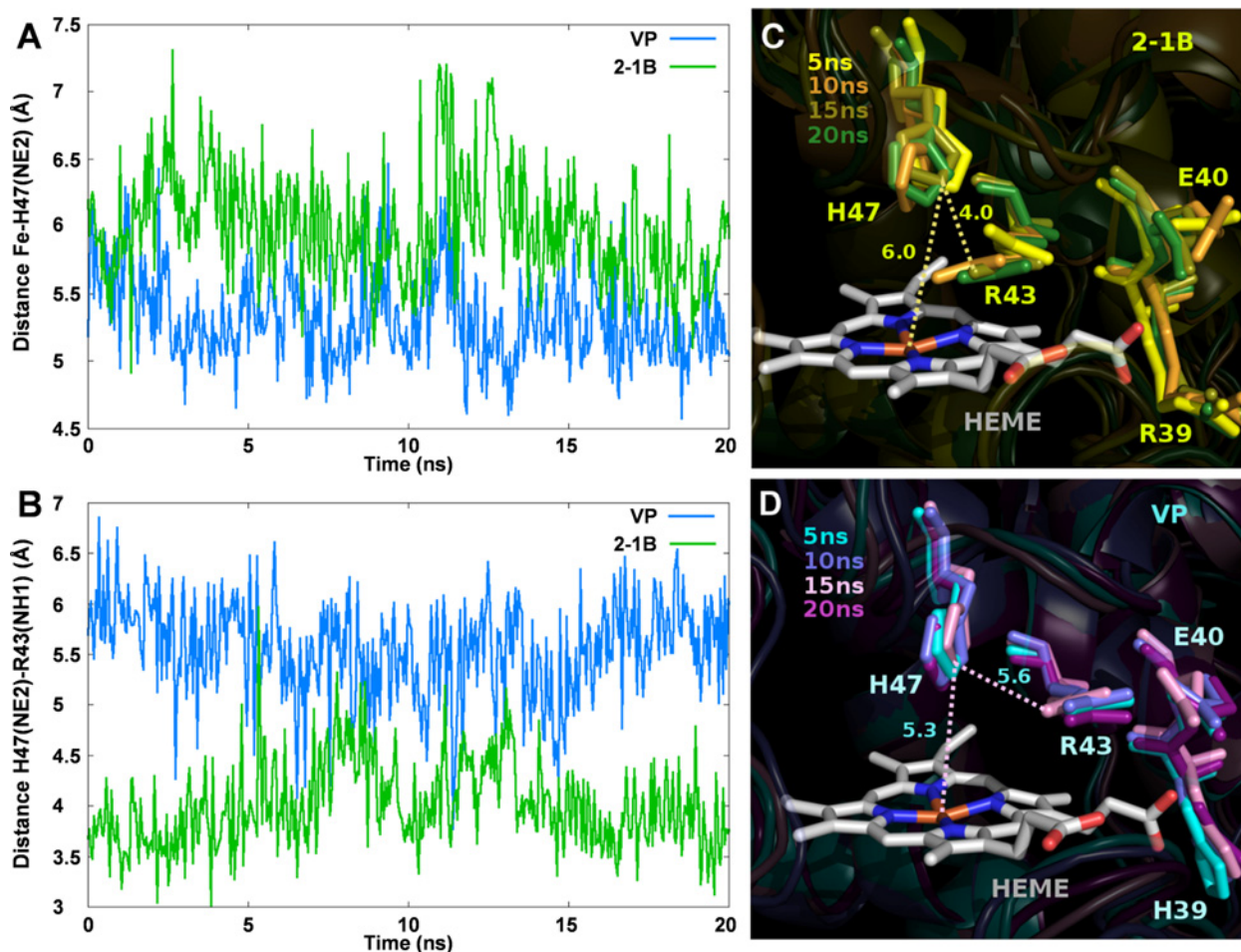


Figure 6 Molecular dynamics simulations

Distance profiles between the haem iron and the distal His-47 (A) and between the distal His-47 and Arg-43 (B); and representative snapshots, with the average distances, extracted from the MD simulations of 2-1B (C) and native VP (D). All distances are in Å.

Molecular dynamics

Taking advantage of the solved crystal structures, the dynamics of native VP and 2-1B in solution were studied by MD simulations at pH 8. Since alkaline inactivation has been related to the formation of a hexa-co-ordinated iron complex with the distal histidine residue, we monitored the evolution of this distance aiming at possible correlations with the stability of the enzyme. Figure 6(A) shows the iron to His-47 distance along a 20 ns MD for both enzymes. Although this distance is similar in both crystals, the addition of thermal fluctuations at room temperature reveals a different behaviour, with a higher distance (~ 1 Å difference on average) for the 2-1B variant. Such distance elongation is the result of a new hydrogen bond between Arg-43 and His-47 (Figure 6C), which is not formed in native VP because of the greater distance between these two residues (Figures 6B and 6D). Overall, inspection of the simulated trajectory indicates a slight shift (along with a higher mobility) in the Arg-43 position, facilitating its interaction with His-47. This deviation towards the histidine residue is mainly due to the electrostatic repulsion produced by the introduction of three new positive residues in the propionate region (E37K, H39R and G330R). In addition, the H39R mutant introduces a stronger interaction with Glu-40, weakening the contact of this glutamic acid with Arg-43.

In native VP, Arg-43 interacts mostly with Glu-40, keeping it away from His-47 and allowing a closer distance of the distal histidine with the haem iron, facilitating the inactivation of the enzyme.

DISCUSSION

The 2-1B variant of *P. eryngii* VP contains seven mutations, introduced during the evolution process in *S. cerevisiae*, that conferred, among other properties, significantly improved alkaline stability, thermostability and enhanced activity on some low-redox-potential substrates [14]. In the present study, we identified some of the structural basis of the alkaline stabilization of this VP variant, by analysing the stability at basic pH and catalytic properties of a series of (single and multiple) variants expressed in *E. coli*.

First, we confirmed that 2-1B expressed in *E. coli* retains the improved properties in terms of alkaline stability and activity at acid pH on low-redox-potential compounds observed when expressed in *S. cerevisiae*. Although the mutations present in 2-1B also contributed to improve the enzyme thermostability when expressed in this eukaryotic host, no differences between 2-1B and native VP were observed when both enzymes were

produced in *E. coli* (results not shown). These results suggest that additional factors contribute to the thermostability improvement in the evolved variant secreted by *S. cerevisiae*. Unlike what was observed for thermostability, 2-1B produced in *E. coli* showed a significantly increased alkaline stability (retaining 80% and 20% activity after 120 h at pH 8 and pH 9 respectively) compared with native VP (which was completely inactivated), although this improvement was not as high as what was found when the variant was expressed in *S. cerevisiae* (100% and 60% activity at pH 8 and pH 9 respectively) [14]. These differences in both thermostability and alkaline stability are likely to be due to the lack of glycosylation of enzymes expressed in *E. coli*, as reported for temperature stability of *Phanerochaete chrysosporium* ligninolytic peroxidases [28]. In general, glycosylation has been described to give robustness and protection against enzyme inactivation [29,30] and could therefore improve the thermostability of yeast-expressed 2-1B and reinforce the alkaline-stabilizing effect of the mutations introduced in this evolved variant.

Explaining the alkaline stability

During alkaline inactivation, ligninolytic peroxidases lose the structural Ca^{2+} ions responsible for maintaining the architecture of the haem environment. This loss leads to a relaxation of the protein structure and hexa-co-ordination of the haem involving the distal histidine residue [31]. These changes are reflected in the electronic absorption spectrum, which is indicative of the high- or low-spin states of the haem iron and its co-ordination state [32]. The *P. eryngii* native VP was inactivated in 24 h upon alkaline incubation (pH 8), showing the spectrum of a low-spin hexa-co-ordinated haem iron. This is characterized by the red-shifted Soret band and the appearance of the α and β bands. Similar changes have been reported for *Bjerkandera adusta* VP [33] and other ligninolytic peroxidases, such as LiP [31] and MnP [32] from *P. chrysosporium*. In contrast, the EHG variant showed improved alkaline stability and conserved the UV-visible spectrum (including the Soret maximum and the CT1 and CT2 bands) unchanged during incubation at pH 8. This spectrum is indicative of a peroxidase with a high-spin ferric state of the haem iron, which is completely functional [34,35]. From these data, it can be inferred that the three new basic residues present in EHG (Lys-37, Arg-39 and Arg-330) reinforced the haem environment enabling the maintenance of penta-co-ordinated haem iron at pH 8.

The stability improvement achieved with the simultaneous introduction of these basic residues could be rationalized by comparative structural analysis and MD simulations of the EHG, 2-1B and native VP crystal structures. The new Arg-39 appeared to be hydrogen-bonded to the haem-distal propionate in the molecular structure of the two variants. The connections of the haem with the apoprotein have been described as being essential for stability [36,37] and engineering new connections with the haem has been proposed as a strategy to increase stability [38]. The haem in ligninolytic peroxidases is non-covalently bound and shows no polar interactions with the apoprotein, with the exception of those that the propionates make. So, the new connection made by Arg-39 seems to be important for the stability achieved, as it anchors the haem to the protein (helix B) and contributes to fix the relative position of His-47 with respect to the iron ion.

On the other hand, the new Lys-37 forms new electrostatic interactions. These interactions have been positively correlated with stability in different families of proteins [39–42]. Those of

Lys-37 with Glu-36 and Glu-83 in EHG and with Glu-40 in 2-1B reinforced the structure of helix B, located directly above the haem and harbouring distal histidine (His-47) and arginine (Arg-43) residues, which are essential in the reaction of the enzyme with H_2O_2 [43] and in the stabilization of the oxidized forms of the haem iron [44,45]. Moreover, as in the case of H39R mutation, fixing the helix B position reduces the possibilities of His-47 to approach the haem and generate the inactive form with hexa-co-ordinated iron. Helix B also contains Asp-48, one of the residues co-ordinating the distal calcium, which is required for pH stability. In addition, a high number of acidic residues were observed around residue 37. At alkaline pH 8, these residues would be deprotonated. In consequence, a high negative charge would characterize this region. The introduction of a basic residue (Lys-37) would reduce the negative charge avoiding detrimental interactions and reinforcing the structure of VP at alkaline pH. At acidic pH, however, the acidic residues will be protonated and no accumulation of negative charge would be produced, explaining the lack of acidic stability improvement of EHG and 2-1B.

The G330R mutation also contributed to the improved stability found in 2-1B and EHG. Although the role played by Arg-330 could not be studied in the crystal structures, it is likely that this residue is located in the same area as residues 37 and 39 and forms new interactions stabilizing the surrounding region containing a high number of acidic residues.

It was remarkable that the stabilizing effect produced by Lys-37, Arg-39 and Arg-330 was only detected when they appeared together, since the H39R variant was unstable and the E37K/G330R variant showed a similar stability to that of the native VP. The sum of the new interactions formed by these residues results in the stabilization of VP, but, individually, they make the protein unstable due to the vulnerability of the region where they are (near the haem and the Mn^{2+} -binding site), being a clear effect of positive epistasis unveiled by directed evolution [14]. According to the structural analysis described above, this effect is caused by the three basic residues simultaneously contributing to stabilize the relative position of the distal histidine. The MD simulations performed under alkaline conditions were quite enlightening in this regard. They revealed that the electrostatic repulsion, formed as a consequence of the introduction of Lys-37, Arg-39 and Arg-330, along with other interactions in which these and other surrounding residues are involved, is able to maintain the distal histidine for longer in a position far enough from the porphyrin to keep the haem iron in a penta-co-ordinate active state.

The EHGQ variant showed higher stability than EHG and almost achieved the alkaline stability found in 2-1B, so it was concluded that: (i) the Q202L mutation also contributed to the enzyme stabilization; and (ii) the four mutations introduced in EHGQ are responsible for the most part of the enhancement towards alkaline stability found in 2-1B. From the analysis of the crystal structure of 2-1B, it was observed that the Q202L substitution promoted the reorganization of Gln-305 and the formation of new interactions in the area which could explain the improvement observed due to this mutation. Although residue 202 is in the core of the protein, the residues affected by the new interactions are solvent-exposed. The solvent-exposed regions are very sensitive to pH changes, so the reinforcement of these areas could be determinantal to strengthening the structure and avoiding the alkaline inactivation at pH 8. Residue 202 would be an example of a residue located far from the haem and the rest of catalytic sites that is able to increase the stability of the enzyme.

Explaining the modified catalytic properties

Regarding the catalytic properties of 2-1B, it was found that this variant is more efficient than the native enzyme oxidizing low-redox-potential substrates, mainly due to an increased affinity (a decreased K_m) in the low-efficiency site. The same behaviour was reported previously for 2-1B expressed in *S. cerevisiae* [14]. With the data in hand, this fact was attributed to the presence of the T184M mutation. It is possible to speculate that the substitution introduced could help with a better substrate accommodation at the main haem-access channel. However, the absence of structural differences in the environment of the residue at position 184 after comparative structural analysis of the native enzyme and 2-1B has not allowed us to give a rational explanation for the effect produced by this mutation on the catalytic activity.

The simultaneous worsening in manganese oxidation is explained by the introduction of Lys-37 and Arg-39 [14]. These two residues could compromise the Mn^{2+} binding by forming electrostatic interactions with Glu-36 and Glu-40 (two of the three residues involved in manganese-co-ordination together with Asp-175) in EHG and 2-1B respectively. Moreover, it is also probable that the new interaction established between the haem internal propionate and the apoprotein in 2-1B and EHG affects the Mn^{2+} binding and oxidation, considering that this propionate is involved in these two events [46]. Interestingly, the kinetic constants for Mn^{2+} oxidation in 2-1B and the rest of the variants were similar to those obtained for VP E36D and E40D variants [46], which suffered a shortening of the lateral chain of Glu-36 and Glu-40 (replacement by aspartic acid). These substitutions led to a worsening in the Mn^{2+} oxidation reflected in a high increase (25-fold) of the K_m and a consequent decrease in the efficiency. In the same way, 2-1B and derived variants showed K_m values 43–54-fold higher. It is likely that electrostatic interactions with Lys-37 in EHG and 2-1B were limiting the mobility of Glu-36 and Glu-40, leading to an impaired activity towards manganese in a similar way to that which happened with the E36D and E40D variants. Finally, substrate oxidation at the catalytic tryptophan residue was not impaired by the mutations introduced in 2-1B given that the oxidation of high-redox compounds such as VA and RB5 by this variant was similar to that found in native VP. This is indicative of the maintenance of the high redox potential of the enzyme, determined by the position of the proximal histidine residue and by the strength of the interaction between this residue and the haem iron [47,48].

Conclusions

We were able to provide a structural–functional basis for the improved alkaline stability of the 2-1B variant by designing and characterizing several (individual and multiple) intermediate variants with the same mutations found in 2-1B. The *E. coli* expression system used not only facilitated variant generation by site-directed mutagenesis, but also enabled crystallization of the non-glycosylated forms of two of them. In this way, the introduction of three basic residues in VP (Lys-37, Arg-39 and Arg-330) resulted in new interactions at the haem environment that avoided the hexa-co-ordination of the haem iron, which leads to enzyme destabilization at pH 8. Moreover, the reinforcement of the solvent-exposed area around Gln-305, in the proximal side, further enhanced the stability. Interestingly, the biochemical characterization of the intermediate variants revealed discrete stability improvements, and the combination of most of them was required to stabilize VP. This stabilization could be obtained by random combination of mutations using directed molecular evolution, and would be impossible by a rational approach since

the basis for the synergistic improvements observed could not be predicted *a priori*. Once VP has been stabilized at alkaline pH, the next step to exploit this new property in industrial applications should be to make the enzyme active at this pH (the optimum of 2-1B and native VP is between pH 3 and 5 for the different substrates that they are able to oxidize [14,17], and no activity at alkaline pH has been observed). Directed evolution approaches are currently being explored to attain this objective with very promising results.

AUTHOR CONTRIBUTION

Verónica Sáez-Jiménez performed most of the experimental biochemical work. Sandra Acebes and Victor Guallar contributed to the MD analyses. Francisco Medrano and Antonio Romero crystallized VP variants. All authors participated in the interpretation and discussion of results. Verónica Sáez-Jiménez, Angel Martínez and Francisco Ruiz-Dueñas contributed data integration and writing.

FUNDING

This work was supported by HIPOP [grant number BIO2011-26694], NOESIS [grant number BIO2014-56388-R] and DEWRY [grant number BIO2013-43407-R] projects of the Spanish Ministry of Economy and Competitiveness (MINECO), and by the PEROXICATS [grant number KBBE-2010-4-265397] and INDOX [grant number KBBE-2013-7-613549] European projects. V.S.-J. and F.J.R.-D. are grateful for the financial support of an FPI fellowship and a Ramón y Cajal contract of the Spanish MINECO, respectively.

REFERENCES

- Ragauskas, A.J., Beckham, G.T., Biddy, M.J., Chandra, R., Chen, F., Davis, M.F., Davison, B.H., Dixon, R.A., Gilna, P., Keller, M. et al. (2014) Lignin valorization: improving lignin processing in the biorefinery. *Science* **344**, 1246843 [CrossRef PubMed](#)
- Martínez, A.T., Ruiz-Dueñas, F.J., Martínez, M.J., del Río, J.C. and Gutiérrez, A. (2009) Enzymatic delignification of plant cell wall: from nature to mill. *Curr. Opin. Biotechnol.* **20**, 348–357 [CrossRef PubMed](#)
- Ruiz-Dueñas, F.J. and Martínez, A.T. (2009) Microbial degradation of lignin: how a bulky recalcitrant polymer is efficiently recycled in nature and how we can take advantage of this. *Microb. Biotechnol.* **2**, 164–177 [CrossRef PubMed](#)
- Martínez, A.T., Speranza, M., Ruiz-Dueñas, F.J., Ferreira, P., Camarero, S., Guillén, F., Martínez, M.J., Gutiérrez, A. and del Río, J.C. (2005) Biodegradation of lignocelluloses: microbiological, chemical and enzymatic aspects of fungal attack to lignin. *Int. Microbiol.* **8**, 195–204 [PubMed](#)
- Floudas, D., Binder, M., Riley, R., Barry, K., Blanchette, R.A., Henrissat, B., Martínez, A.T., Otililar, R., Spatafora, J.W., Yadav, J.S. et al. (2012) The Paleozoic origin of enzymatic lignin decomposition reconstructed from 31 fungal genomes. *Science* **336**, 1715–1719 [CrossRef PubMed](#)
- Hammel, K.E. and Cullen, D. (2008) Role of fungal peroxidases in biological ligninolysis. *Curr. Opin. Plant Biol.* **11**, 349–355 [CrossRef PubMed](#)
- Gold, M.H., Youngs, H.L. and Gelpke, M.D. (2000) Manganese peroxidase. *Met. Ions Biol. Syst.* **37**, 559–586 [PubMed](#)
- Fernández-Fueyo, E., Acebes, S., Ruiz-Dueñas, F.J., Martínez, M.J., Romero, A., Medrano, F.J., Guallar, V. and Martínez, A.T. (2014) Structural implications of the C-terminal tail in the catalytic and stability properties of manganese peroxidases from ligninolytic fungi. *Acta Crystallogr. D Biol. Crystallogr.* **70**, 3253–3265 [CrossRef PubMed](#)
- Ruiz-Dueñas, F.J., Morales, M., García, E., Miki, Y., Martínez, M.J. and Martínez, A.T. (2009) Substrate oxidation sites in versatile peroxidase and other basidiomycete peroxidases. *J. Exp. Bot.* **60**, 441–452 [CrossRef PubMed](#)
- Morales, M., Mate, M.J., Romero, A., Martínez, M.J., Martínez, A.T. and Ruiz-Dueñas, F.J. (2012) Two oxidation sites for low redox-potential substrates: a directed mutagenesis, kinetic and crystallographic study on *Pleurotus eryngii* versatile peroxidase. *J. Biol. Chem.* **287**, 41053–41067 [CrossRef PubMed](#)
- Martínez, A.T., Ruiz-Dueñas, F.J., Gutiérrez, A., del Río, J.C., Alcalde, M., Liers, C., Ullrich, R., Hofrichter, M., Scheibner, K., Kalum, L. et al. (2014) Search, engineering and applications of new oxidative biocatalysts. *Biofuels Bioprod. Biorefining* **8**, 819–835 [CrossRef](#)
- Ragauskas, A.J., Williams, C.K., Davison, B.H., Britovsek, G., Cairney, J., Eckert, C.A., Frederick, W.J., Hallett, J.P., Leak, D.J., Liotta, C.L. et al. (2006) The path forward for biofuels and biomaterials. *Science* **311**, 484–489 [CrossRef PubMed](#)

- 13 Husain, Q. (2010) Peroxidase mediated decolorization and remediation of wastewater containing industrial dyes: a review. *Rev. Environ. Sci. Bio.* **9**, 117–140 [CrossRef](#)
- 14 García-Ruiz, E., González-Pérez, D., Ruiz-Dueñas, F.J., Martínez, A.T. and Alcalde, M. (2012) Directed evolution of a temperature-, peroxide- and alkaline pH-tolerant versatile peroxidase. *Biochem. J.* **441**, 487–498 [CrossRef PubMed](#)
- 15 Sambrook, J. and Russell, D.W. (2001) *Molecular Cloning*, Cold Spring Harbor Laboratory Press, Cold Spring Harbor
- 16 Pérez-Boada, M., Doyle, W.A., Ruiz-Dueñas, F.J., Martínez, M.J., Martínez, A.T. and Smith, A.T. (2002) Expression of *Pleurotus eryngii* versatile peroxidase in *Escherichia coli* and optimisation of *in vitro* folding. *Enzyme Microb. Technol.* **30**, 518–524 [CrossRef](#)
- 17 Ruiz-Dueñas, F.J., Martínez, M.J. and Martínez, A.T. (1999) Molecular characterization of a novel peroxidase isolated from the ligninolytic fungus *Pleurotus eryngii*. *Mol. Microbiol.* **31**, 223–236 [CrossRef PubMed](#)
- 18 Britton, H.T.S. and Robinson, R.A. (1931) Universal buffer solutions and the association constant of veronal. *J. Chem. Soc.* 1456–1462 [CrossRef](#)
- 19 Kabsch, W. (2010) XDS. *Acta Crystallogr. Sect. D Biol. Crystallogr.* **66**, 125–132 [CrossRef](#)
- 20 Adams, P.D., Afonine, P.V., Bunkoczi, G., Chen, V.B., Davis, I.W., Echols, N., Headd, J.J., Hung, L.W., Kapral, G.J., Grosse-Kunstleve, R.W. et al. (2010) PHENIX: a comprehensive Python-based system for macromolecular structure solution. *Acta Crystallogr. Sect. D Biol. Crystallogr.* **66**, 213–221 [CrossRef](#)
- 21 Emsley, P., Lohkamp, B., Scott, W.G. and Cowtan, K. (2010) Features and development of Coot. *Acta Crystallogr. Sect. D Biol. Crystallogr.* **66**, 486–501 [CrossRef](#)
- 22 Chen, V.B., Arendall, W.B., Headd, J.J., Keedy, D.A., Immormino, R.M., Kapral, G.J., Murray, L.W., Richardson, J.S. and Richardson, D.C. (2010) MolProbity: all-atom structure validation for macromolecular crystallography. *Acta Crystallogr. Sect. D Biol. Crystallogr.* **66**, 12–21 [CrossRef](#)
- 23 Davis, I.W., Leaver-Fay, A., Chen, V.B., Block, J.N., Kapral, G.J., Wang, X., Murray, L.W., Arendall, III, W.B., Snoeyink, J., Richardson, J.S. and Richardson, D.C. (2007) MolProbity: all-atom contacts and structure validation for proteins and nucleic acids. *Nucleic Acids Res.* **35**, W375–W385 [CrossRef PubMed](#)
- 24 Sastry, G.M., Adzhigirey, M., Day, T., Annabhimoju, R. and Sherman, W. (2013) Protein and ligand preparation: parameters, protocols, and influence on virtual screening enrichments. *J. Comput. Aided Mol. Des.* **27**, 221–234 [CrossRef PubMed](#)
- 25 Kaminski, G.A., Friesner, R.A., Tirado-Rives, J. and Jorgensen, W.L. (2001) Evaluation and reparametrization of the OPLS-AA force field for proteins via comparison with accurate quantum chemical calculations on peptides. *J. Phys. Chem. B* **105**, 6474–6487 [CrossRef](#)
- 26 Nosé, S. (1984) A unified formulation of the constant temperature molecular dynamics methods. *J. Chem. Phys.* **81**, 511–519 [CrossRef](#)
- 27 Martyna, G.J., Tobias, D.J. and Klein, M.L. (1994) Constant pressure molecular dynamics algorithms. *J. Chem. Phys.* **101**, 4177–4189 [CrossRef](#)
- 28 Nie, G.J., Reading, N.S. and Aust, S.D. (1999) Relative stability of recombinant versus native peroxidases from *Phanerochaete chrysosporium*. *Arch. Biochem. Biophys.* **365**, 328–334 [CrossRef PubMed](#)
- 29 Olden, K., Bernard, B.A., Humphries, M.J., Yeo, T.K., Yeo, K.T., White, S.L., Newton, S.A., Bauer, H.C. and Parent, J.B. (1985) Function of glycoprotein glycans. *Trends Biochem. Sci.* **10**, 78–82 [CrossRef](#)
- 30 Tams, J.W. and Welinder, K.G. (1998) Glycosylation and thermodynamic versus kinetic stability of horseradish peroxidase. *FEBS Lett.* **421**, 234–236 [CrossRef PubMed](#)
- 31 George, S.J., Kvaratskhelia, M., Dilworth, M.J. and Thorneley, R.N.F. (1999) Reversible alkaline inactivation of lignin peroxidase involves the release of both the distal and proximal site calcium ions and bishistidine co-ordination of the haem. *Biochem. J.* **344**, 237–244 [CrossRef PubMed](#)
- 32 Youngs, H.L., Moënne-Loccoz, P., Loehr, T.M. and Gold, M.H. (2000) Formation of a bis(histidyl) heme iron complex in manganese peroxidase at high pH and restoration of the native enzyme structure by calcium. *Biochemistry* **39**, 9994–10000 [CrossRef PubMed](#)
- 33 Verdín, J., Pogni, R., Baeza, A., Baratto, M.C., Basosi, R. and Vázquez-Duhalt, R. (2006) Mechanism of versatile peroxidase inactivation by Ca²⁺ depletion. *Biophys. Chem.* **121**, 163–170 [CrossRef PubMed](#)
- 34 Pérez-Boada, M., Ruiz-Dueñas, F.J., Pogni, R., Basosi, R., Choinowski, T., Martínez, M.J., Piontek, K. and Martínez, A.T. (2005) Versatile peroxidase oxidation of high redox potential aromatic compounds: site-directed mutagenesis, spectroscopic and crystallographic investigations of three long-range electron transfer pathways. *J. Mol. Biol.* **354**, 385–402 [CrossRef PubMed](#)
- 35 Santoni, E., Jakopitsch, C., Obinger, C. and Smulevich, G. (2004) Comparison between catalase-peroxidase and cytochrome *c* peroxidase: the role of the hydrogen-bond networks for protein stability and catalysis. *Biochemistry* **43**, 5792–5802 [CrossRef PubMed](#)
- 36 Henriksen, A., Mirza, O., Indiani, C., Teilum, K., Smulevich, G., Welinder, K.G. and Gajhede, M. (2001) Structure of soybean seed coat peroxidase: a plant peroxidase with unusual stability and haem-apoprotein interactions. *Protein Sci.* **10**, 108–115 [CrossRef PubMed](#)
- 37 Mirza, O., Henriksen, A., Ostergaard, L., Welinder, K.G. and Gajhede, M. (2000) *Arabidopsis thaliana* peroxidase N: structure of a novel neutral peroxidase. *Acta Crystallogr. Sect. D Biol. Crystallogr.* **56**, 372–375 [CrossRef](#)
- 38 Kamal, J.K.A. and Behere, D.V. (2008) Kinetic stabilities of soybean and horseradish peroxidases. *Biochem. Eng. J.* **38**, 110–114 [CrossRef](#)
- 39 Vogt, G., Woell, S. and Argos, P. (1997) Protein thermal stability, hydrogen bonds, and ion pairs. *J. Mol. Biol.* **269**, 631–643 [CrossRef PubMed](#)
- 40 Kumar, S., Tsai, C.J. and Nussinov, R. (2000) Factors enhancing protein thermostability. *Protein Eng.* **13**, 179–191 [CrossRef PubMed](#)
- 41 Vinther, J.M., Kristensen, S.M. and Led, J.J. (2011) Enhanced stability of a protein with increasing temperature. *J. Am. Chem. Soc.* **133**, 271–278 [CrossRef PubMed](#)
- 42 Gromiha, M.M., Pathak, M.C., Saraboji, K., Ortlund, E.A. and Gaucher, E.A. (2013) Hydrophobic environment is a key factor for the stability of thermophilic proteins. *Proteins* **81**, 715–721 [CrossRef PubMed](#)
- 43 Hiner, A.N.P., Raven, E.L., Thorneley, R.N.F., García-Canovas, F. and Rodríguez-López, J.N. (2002) Mechanisms of compound I formation in heme peroxidases. *J. Inorg. Biochem.* **91**, 27–34 [CrossRef PubMed](#)
- 44 Erman, J.E., Vitello, L.B., Miller, M.A., Shaw, A., Brown, K.A. and Kraut, J. (1993) Histidine 52 is a critical residue for rapid formation of cytochrome *c* peroxidase compound I. *Biochemistry* **32**, 9798–9806 [CrossRef PubMed](#)
- 45 Vitello, L.B., Erman, J.E., Miller, M.A., Wang, J. and Kraut, J. (1993) Effect of Arginine-48 replacement on the reaction between cytochrome *c* peroxidase and hydrogen peroxide. *Biochemistry* **32**, 9807–9818 [CrossRef PubMed](#)
- 46 Ruiz-Dueñas, F.J., Morales, M., Pérez-Boada, M., Choinowski, T., Martínez, M.J., Piontek, K. and Martínez, A.T. (2007) Manganese oxidation site in *Pleurotus eryngii* versatile peroxidase: a site-directed mutagenesis, kinetic and crystallographic study. *Biochemistry* **46**, 66–77 [CrossRef PubMed](#)
- 47 Banci, L., Camarero, S., Martínez, A.T., Martínez, M.J., Pérez-Boada, M., Pierattelli, R. and Ruiz-Dueñas, F.J. (2003) NMR study of Mn(II) binding by the new versatile peroxidase from the white-rot fungus *Pleurotus eryngii*. *J. Biol. Inorg. Chem.* **8**, 751–760 [CrossRef PubMed](#)
- 48 Banci, L., Bertini, I., Turano, P., Tien, M. and Kirk, T.K. (1991) Proton NMR investigation into the basis for the relatively high redox potential of lignin peroxidase. *Proc. Natl. Acad. Sci. U.S.A.* **88**, 6956–6960 [CrossRef PubMed](#)

Received 4 January 2016/22 April 2016; accepted 26 April 2016
Accepted Manuscript online 26 April 2016, doi:10.1042/BCJ20160248